



The Influence of Impeller Design on Hydraulic Performance of Vortex Pump

Hadi Fallah Ardeshir ^{a,*}, Tohid Javadpour ^b

^a Assistant Professor, Faculty of Mechanical Engineering, Sahand University of Technology, Tabriz, Iran

^b Ms.c, Faculty of Mechanical Engineering, Sahand University of Technology, Tabriz, Iran

ARTICLE INFO

Article history:

Received 05 May 2025

Received in revised form 21 May 2025

Accepted 24 May 2025

Available online 24 May 2025

Keywords:

Vortex Pump

Pump Impeller

Pump Efficiency

Impeller Blade

Pump Head

Numerical Simulation

ABSTRACT

This study investigates the performance of vortex pumps by focusing on impeller design to improve efficiency and operational capabilities. Vortex pumps are valuable in industries that handle fluids containing solids including wastewater treatment and mining due to their clog-resistant design. However, these pumps often suffer from lower efficiency compared to centrifugal pumps. To address this issue, the study employs Computational Fluid Dynamics (CFD) simulations to analyze various impeller configurations including adjustments to blade count, shape and height. The simulations reveal that a 12-blade impeller configuration significantly enhances pump performance, achieving an increase in head by 4.85 meters and efficiency by 5.46% over the baseline design. These findings provide valuable insights for the vortex pump design, emphasizing that blade configuration especially blade count and angle has a more significant effect on performance than blade height. The results encourage the use of modified impellers to enhance energy efficiency and longevity in industrial applications involving solid-laden fluids.

1. Introduction

Handling mixtures of solid materials and liquids presents significant challenges, especially in industries including wastewater treatment, mining and food processing. Solid particles in fluids can lead to clogging, abrasion and mechanical strain on equipment which reduces efficiency and increase maintenance costs. Conventional centrifugal pumps often have difficulty handling such mixtures effectively, as they are sensitive to blockages when dealing with larger particles or fluids with high solid content. One solution to this problem is the use of vortex pumps. These types of pumps, which have often called "free-flow pump, sludge pump and Torque Flow Pump (TFP) due

* Corresponding author.

E-mail addresses: fallah.hadi@sut.ac.ir (H. Fallah Ardeshir)

to their efficiency, are known for their high resistance to clogging and robust performance [1]. Vortex pumps are designed with a special chamber structure that allows them to handle liquids containing large particles with minimal blockages. Creating a strong rotational flow, allows these pumps move solids more freely through the chamber, reducing wear and tear on the pump components. As industries continue to develop, adopting vortex pumps for solid-fluid transportation offers a practical approach to enhance operational efficiency and extend the longevity of pumping systems [2]. Because of the large space between the volute and the impeller, vortex pumps have excellent anti-clogging performance and often work better than centrifugal pumps. With the ongoing development of industry and agriculture, these pumps are now widely used in areas such as sewage treatment, slurry handling, and transporting media with large particles [3]. In vortex pumps, two flow patterns can be observed in the non-blade cavity: through-flow and circulation flow. Typically, the efficiency of these pumps is below 60%, primarily due to the presence of circulation flow [4]. Additionally, these pumps face challenges like high energy consumption, partial clogging, and excessive wear when transporting solid materials. Given the importance of energy conservation, enhancing the performance of vortex pumps appears to be desirable. Meanwhile, this improvement must maintain the ability of pump to handle liquids containing solid particles. Currently, due to the limited information available on the operation of vortex pumps, the optimal design for achieving maximum efficiency is not clear. To address these issues, numerous studies have focused on optimizing their design. In 1954, the first vortex pump was made by the Western Machine Company, and then a company in Sweden experimentally produced the vortex pump for the first time [5]. In the 1980s, Schivley introduced the first flow model, assuming steady, symmetric flow with parameters dependent only on the radius. He developed a one-dimensional analytical model to analyze the pump; however, the actual flow was more complex than a simple one-dimensional representation [6]. In 1983, Ohba et al. investigated various geometrical parameters of vortex pumps to determine the optimal design [7]. Gerlach et al. examined how variations in geometric parameters affect the characteristics of vortex pumps [8]. Additionally, they conducted a numerical study of the internal flow field within a vortex pump, comparing their findings to the Hamel–Oseen vortex model. Their research shows that a vortex similar to the Hamel–Oseen vortex forms only under significant part-load conditions. [9]. In reality, there are two distinct design approaches based on different assumptions: the closed design and the open design [10]. In the closed design, the radial and outer sections of the impeller are contained within the casing, which is assumed to play a crucial role in fluid transfer. The working principle involves the impeller creating a vortex in the front chamber, which helps to improve fluid movement. In the open design, the configuration allows the fluid to flow freely in the external environment of the impeller. Essentially, it is assumed that the vortex pump operates similarly to centrifugal pumps, meaning that the fluid is directly pumped through the impeller itself. The vortex is primarily a result of the pressure losses from the high-pressure side to the low-pressure side, which accounts for the relatively low hydraulic efficiency of vortex pumps [11–13]. Li et al. employed a numerical calculation method to investigate a centrifugal pump equipped with a vane diffuser. They extracted and analyzed the vortex structure at the vane passing frequency and used the Q-criterion to identify the horseshoe vortex. Their results showed that the main regions of vortex concentration were at the impeller outlet, the diffuser trailing edge and near the volute tongue. [14]. Yi Li et al. developed a unified algorithm combining Short-Time Fourier Transform (STFT) and Wigner-Ville Distribution (WVD) to analyze the time-frequency characteristics of cavitation phenomena that lead to pump instability. This method improves the detection and assessment of the pump's cavitation performance. [15]. Another approach to

examining the performance and optimizing vortex pumps is to analyze the flow generated within the pump's volute. The volute of a vortex pump plays a crucial role in its performance, particularly in managing flow dynamics and pressure characteristics. The design and of the volute can significantly influence to the efficiency of the pump, pressure pulsation and overall operational stability. Below are key aspects of the volute's function and design considerations [16]. Sha et al. observed the flow inside a vortex pump through a transparent casing and found that the flow can be divided into two components: through-flow and vortex flow [17]. While experimental results are reliable, testing often requires significant financial and time resources. Consequently, more efficient research methods are required. Therefore, with the advancement of computers and the science of Computational Fluid Dynamics (CFD), researchers started to solve the time-averaged Reynolds equation with turbulence models. The investigation of the pump's internal flow field has advanced into the era of three-dimensional numerical simulation. The main turbulence simulation methods used are Direct Numerical Simulation (DNS), Large Eddy Simulation (LES), and Reynolds-Averaged Navier-Stokes (RANS). Another crucial component of the vortex pump that plays an essential role in its performance is the impeller. In vortex pumps, various impellers are used depending on the type and efficiency of the pump. Different parameters can be applied to the impellers including the number of blades, the outlet angle of the blades, the diameter of the impeller, the width of the impeller, bowl-shaped impellers, adding partial blades and increasing or decreasing the blade height at different points [18]. The main goal is to design an impeller with the best combination of parameters adapted to the requirements of the pump, to ensure it achieves the desired performance. In a study of propellers with straight blades, three designs were tested in water: 12, 8, and 14 blades, each with a diameter of 240 mm and a blade depth of 3.40 mm. Results showed that while the pressure and power coefficients slightly increased with more blades, the efficiency was highest for the 12-blade propeller at 3.47%. The 14-blade propeller followed at 2.47%, and the 8-blade impeller had the lowest efficiency at 6.46%. Overall, the 12-blade design was preferred for its superior efficiency despite the minimal pressure coefficient improvement from 12 to 14 blades [19]. Zhao et al. concluded that the impeller's installation position significantly impacts the hydraulic performance and unsteady flow characteristics of a vortex pump, affecting circulation flow and pressure pulsation levels [20]. Quan et al. optimized the overall blade structure of a vortex pump using the orthogonal test method to clarify the matching relationship between the impeller and casing structures, thereby improving the hydraulic performance of vortex pump [21]. Gao et al. has designed two types of vortex pump impellers with different blade wrap angles and evaluated their external characteristics and internal flow fields under varying flow rates [22]. Jiang and Wang conducted a study to investigate the energy loss mechanisms in centrifugal pump impellers using numerical simulation. The research focuses on the behavior of vortices under different viscosities and rotational speeds. The results indicate that at low viscosities, turbulent dissipation is the primary contributor to entropy production [23]. J. Yang and X. Li conducted an investigation of the internal flow characteristics of a vortex pump using numerical simulation, with the results validated against experimental data to ensure accuracy. Based on this validated model, they applied the orthogonal design method to optimize the impeller structure. The optimized design led to a significant improvement in the overall performance of the vortex pump [24]. Lu Xin et al. investigate the use of machine learning to improve the stability and performance of pump turbine impeller blades. A prognostic model was developed based on blade streamline control variables, utilizing advanced programming and numerical simulation tools for blade optimization. The results show that the optimized blades effectively reduce the formation of high-speed water rings and minimize flow

blockages, leading to a more uniform distribution of turbulent kinetic energy [25]. In another study to optimize vortex pump performance and reduce vibration, the orthogonal testing method was used, focusing on parameters like impeller outer diameter, outlet width, and setting angles. A comprehensive analysis determined the primary and secondary factors affecting performance. The optimized pump showed a 4.2% efficiency increase and a 9m higher head compared to the prototype, validating the numerical calculation method. Backflow was observed at the pump entrance, moving along the pipe wall to the inlet and interacting with the incoming flow [26]. This study presents a comprehensive and systematic investigation into enhancing vortex pump performance through impeller design optimization using advanced CFD techniques. The three-dimensional flow within a vortex pump equipped with a volute has been simulated using SST turbulence model under steady-state conditions. Additionally, a multiple reference frame approach has been used where the impeller operates in a rotating frame and the volute remains stationary. Two impeller designs were analyzed: one with 8 straight blades and another with 12 backward-curved blades. The research identifies the critical design parameters that most significantly impact hydraulic performance. Unlike previous studies that focused on singular design features, this work demonstrates that the number and orientation of impeller blades have a far greater influence on performance than changes in blade height alone.

2. Vortex pump simulation

The studied vortex pump has been used in Mobarakeh Steel to handle solid materials immersed in water, including small and irregular solid particles of mineral iron ore. This pump is powered by a 132-kilowatts electric motor, which transmits power through a belt to the shaft and subsequently to the impeller. The initial geometry of the pump, including volute and impeller, was extracted from the reverse engineering pump of Toro Company and installed by Mobarake Steel Company of Isfahan. The design of the pump is based on a closed design, the outer area of the impeller is enclosed with the pump body and the large distance in front of the impeller to the body has minimized the risk of clogging, and the impeller used has eight straight blades that rotate at a speed of 1230 rpm.

2.1. Pump simulation

The pump casing, commonly referred to as the volute, has an overall width of 383mm. Key specifications include an inlet with a diameter of 250mm, an impeller housing with a diameter of 435mm and a width of 83mm and a front chamber extending 200mm from the impeller to the pump wall. The outlet has a diameter of 198mm. Additionally, the impeller of this pump has a diameter of 426 mm and a base thickness of 17.5 mm. It includes eight straight blades with a height of 56 mm. The pump and impeller have been developed using CATIA software, with dimensions detailed in the Figure 1 and Figure 2.

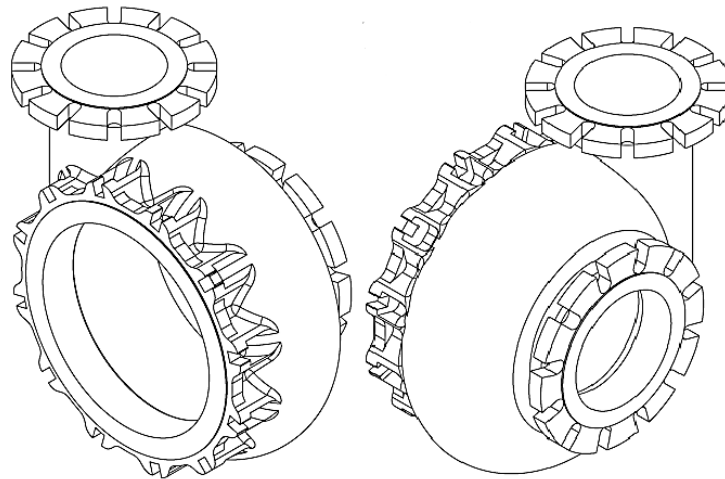


Figure 1. Casing of vortex pump

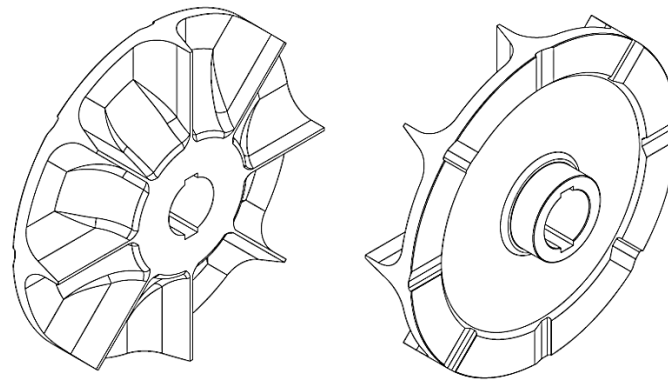


Figure 2. Impeller of vortex pump

The pump impeller rotates at 1230 RPM, moving a fluid that is a mixture of water and irregularly sized iron ore stones. This fluid has a density of 1011 kg/m^3 and exits the pump at a flow rate of $450 \text{ m}^3/\text{h}$. Under these conditions, the pump consumes 110 kW of energy, provides a head of 35 meters, and records an efficiency of approximately 39.40%. The objective of this study is to increase both the head and efficiency of the pump. Table 1 presents all specifications of the vortex pump under study.

Table 1. Characteristics of the studied vortex pump

Power consumption (kw)	Impeller velocity (rpm)	Total head (m)	Output flow rate (m^3/h)	Density (kg/m^3)	Efficiency (%)
110	1230	35	450	1011	39.40

2.2. Geometry simulation

As previously mentioned, vortex pumps generally have lower efficiency compared to other pump types, likely because energy of the impellers is much more dissipated within the rotational flow

rather than being fully transferred to the fluid. Since the impeller is enclosed within the casing, classifying this pump as a closed-type design. It is assumed that the impeller generates a vortex within its front chamber, which in turn facilitates the transfer of fluid containing solid particles. To enhance efficiency, the geometry of the volute and impeller of the reference pump was initially designed and simulated using CATIA and ANSYS CFX software, respectively. Simulation data are used as a criterion for comparing the performance of the modified pump models with the reference design. Following the simulation of the reference vortex pump, modifications were applied to the impeller blades. Subsequently, an alternative impeller of the same diameter but featuring redesigned blades has been replaced with the original impeller. For the simulation, the internal geometry of the pump, where the fluid flows, is required; specifically, the parts of the pump and impeller geometry containing the fluid are essential for accurate simulation. Therefore, it is necessary to obtain the geometry of the internal volute area of the pump and the region between the impeller blades that contain the fluid. After obtaining the desired geometries, the impeller fluid region is positioned within the volute fluid region of the pump. The geometries of the fluid regions and the overall pump are illustrated in the Figure 3.

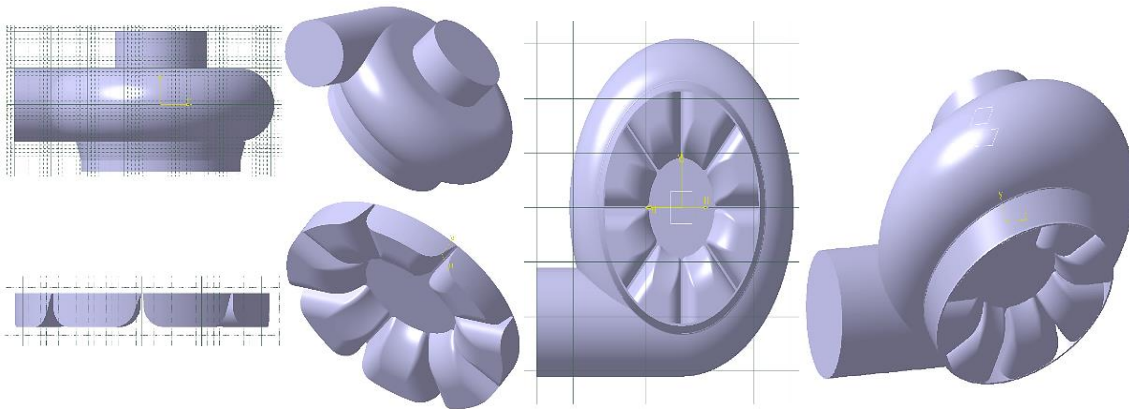


Figure 3. Geometry of the Volute and Impeller Fluid Regions of the Pump

2.3. Geometry meshing

The meshing process in ANSYS software has been used to divide the obtained geometry into smaller elements suitable for numerical analysis. To ensure high-quality results and accurately capture the complex flow behavior within the pump. Two different mesh types were used for the impeller and the volute, based on their geometric complexity and computational demand. For the impeller which has intricate and curved surfaces, a tetrahedral mesh type has been utilized. Tetrahedral meshes are appropriate for complex geometries as they can adapt to irregular shapes and provide superior resolution in areas with sharp curves. This ensures that the flow dynamics around the impeller blades and other intricate features have been accurately represented. On the other hand, the volute which has a relatively simpler and more structured geometry, has been meshed using a hex-dominant mesh type. Hex-dominant meshes have been known for their efficiency in capturing flow behavior in less complex geometries. This approach has reduced the computational cost and has improved solution stability and convergence for structured regions of the geometry. To ensure consistency and perform

a direct comparison in performance of the two meshing methods, a uniform mesh size of 0.05m has been applied to both the impeller and the volute. However, to have reliable numerical results, refine meshing and avoid mesh-dependent divisions, a mesh independency analysis has been conducted. By performing this analysis, the optimal mesh size has been determined to ensure that the simulation results have been both accurate and computationally efficient. The final model of the impeller and volute with their respective mesh types has been illustrated in Figure 4. This figure provides multiple views of the pump meshing and the detailed tetrahedral mesh around the impeller and the structured hex-dominant mesh in the volute region. It highlights the distinct meshing patterns employed to accurately capture the flow behavior in both complex and simpler geometric regions of the pump. The combination of these meshing patterns has ensured that the complex flow behavior within the pump has been accurately captured while maintaining a reasonable computational cost. This approach has been critical for ensuring reliable and precise simulation results in the analysis of pump performance.

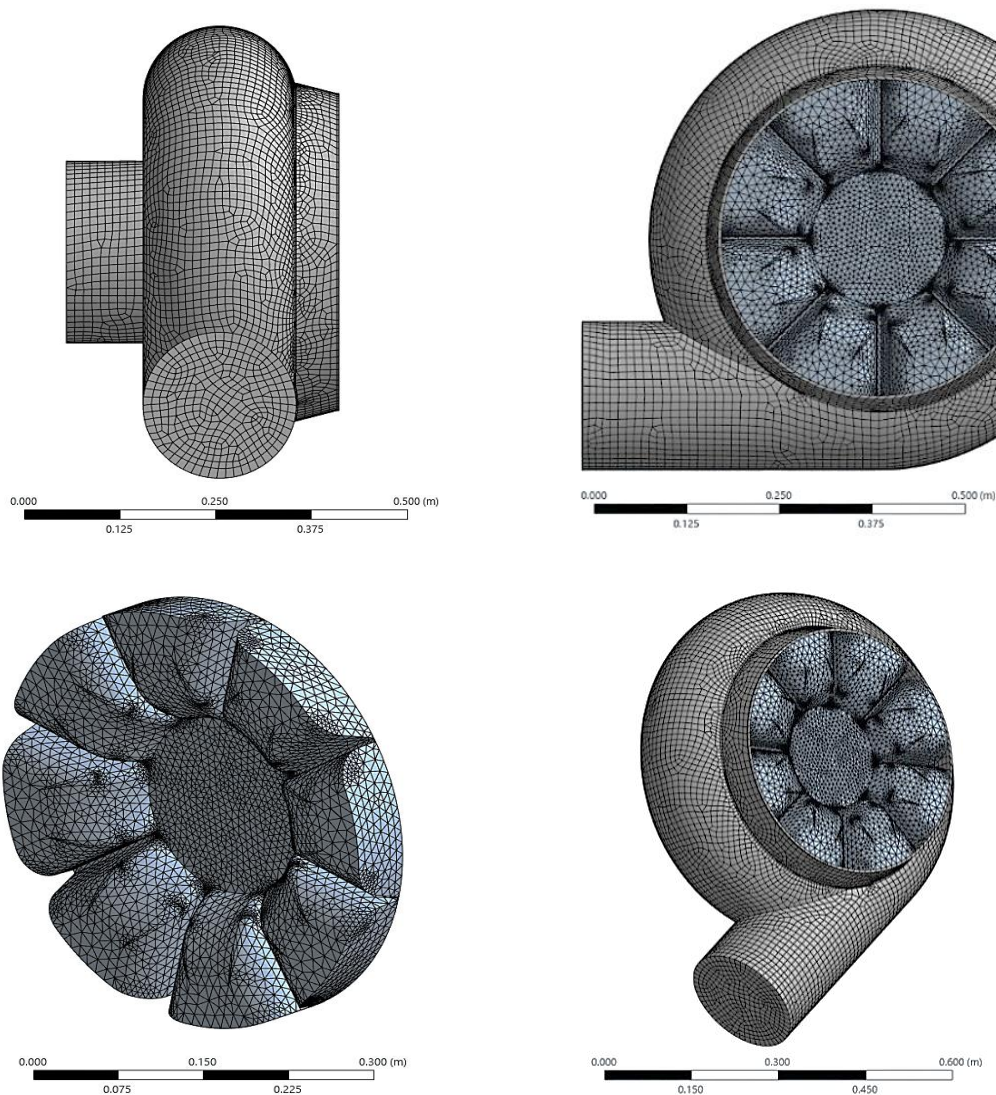


Figure 4. The meshing of the pump volute and impeller

Mesh independence has been verified through a step-by-step process. In this method, mesh sizes have been reduced and simulations have been performed for each refined configuration. The primary objective of this process is to identify the optimal mesh size that effectively balances computational efficiency with the accuracy of the results. The mesh has been refined step by step until further refinement had little or no effect on the simulation results. This ensures that the results are independent of the mesh resolution which demonstrates that the numerical predictions accurately represent the physical behavior without being influenced by mesh errors. The evaluation process focuses on analyzing critical performance parameters including flow characteristics, pressure distributions across crucial components and efficiency metrics (hydraulic efficiency and head loss). These parameters are monitored and compared across simulations with varying mesh sizes to assess convergence behavior. By comparing the results, the point at which successive mesh refinements yield insignificant differences in the outcomes is determined. This convergence point confirms that the results have achieved mesh independence which indicate that they are no longer sensitive to further reductions in mesh size. This procedure enhances the reliability of the numerical model while maintaining computational efficiency by preventing overly fine meshes. Excessive mesh refinement can result in higher computational costs, such as longer simulation times and increased resource usage, without significantly improving accuracy. Hence, the mesh independence study plays a crucial role in optimizing the simulation setup which ensures that the model is both accurate and computationally practical. The findings of the mesh independence study are shown in Table 2 which provides a detailed comparison of the key performance metrics across the different mesh configurations. This table highlights the convergence behavior of the results and identifies the optimal mesh size that achieves the desired balance between accuracy and efficiency. This approach is essential for producing high-quality simulation results that can be used for design optimization, performance analysis and decision-making processes.

Table 2. Characteristics of meshing and head of the pump

# Num	Number of Elements	Number of Nodes	Mesh size (m)	Pump head (m)
1	126729	291330	0.016	37.31
2	144028	335873	0.015	37.66
3	163131	384863	0.014	38.11
4	187647	451429	0.013	38.16
5	201937	488153	0.012	38.18
6	219327	542016	0.011	38.17
7	225781	583259	0.010	38.16

According to Table 2, it can be observed that as the number of elements increases, the calculated head of the vortex pump gradually improves. This indicates that a finer mesh enhances the accuracy of the numerical simulation by better capturing flow characteristics. However, after the mesh size decreases to less than 0.012m, increasing the number of elements no longer significantly affects the performance of the pump. Additionally, the pump head decreases slightly, which might be caused by numerical dissipation or excessive computational errors. Hence, it can be concluded that a mesh size of 0.012m provides the best performance and balancing computational efficiency and solution accuracy.

2.4. Turbulence model

The flow in turbomachines is turbulent due to the high Reynolds number. Hence, turbulence models are essential for accurate flow analysis and the prediction of flow behavior. In steady-state incompressible flow averaging, conservation equations can be solved using Reynolds-averaged values or time-averaged values. These approaches help simplify the complex turbulent flow structures while maintaining accuracy in numerical simulation. Among the various available turbulence models, the K- ε model is the most widely used for solving numerical problems due to the robustness and reliability. This model consists of two transport equations which is defined in equations (1) and (2): one for the turbulent kinetic energy (K) and another for the rate of energy dissipation (ε) which describes the turbulence characteristics of the flow. These equations allow for the prediction of turbulence intensity, the dissipation rate and providing a practical approach to modeling turbulent flows in engineering applications. The K- ε model effectively describes the energy transfer in turbulent eddies and is particularly suitable for industrial applications including turbomachinery and pipe flows. However, it accurately predicts mean flow properties. Nonetheless, it may be difficult to accurately resolve complex flow separations and vortical structures, where more advanced turbulence models like the K- ω model or LES are generally more effective. Despite these limitations, the K- ε model remains an appropriate choice due to the balance between computational cost and accuracy [27].

$$\frac{\partial}{\partial x_j}(\rho \bar{u}_j k) = P_k - \rho \varepsilon + \frac{\partial}{\partial x_j} \left[\left(\mu + \frac{\mu_t}{\sigma_k} \right) \frac{\partial k}{\partial x_j} \right] \quad (1)$$

$$\frac{\partial}{\partial x_j}(\rho \bar{u}_j \varepsilon) = C_{\varepsilon 1} \frac{\varepsilon}{k} P_k - C_{\varepsilon 2} \rho \frac{\varepsilon^2}{k} + \frac{\partial}{\partial x_j} \left[\left(\mu + \frac{\mu_t}{\sigma_\varepsilon} \right) \frac{\partial \varepsilon}{\partial x_j} \right] \quad (2)$$

while \bar{u}_j is the mean velocity component in j direction, P_k represents the production of turbulent kinetic energy, σ_k and σ_ε are the prandtl numbers for k and ε , respectively. $C_{\varepsilon 1}$ and $C_{\varepsilon 2}$ are the empirical constants specific to the K- ε model. Additionally, ρ , u , μ are the density of fluid, velocity, dynamic viscosity of fluid, respectively and μ_t is the turbulent viscosity. Another turbulence model is the K- ω model which is described in **Eq. (3) and (4)**.

$$\frac{\partial}{\partial x_j}(\rho \bar{u}_j k) = P_k - C_\mu \rho k \omega + \frac{\partial}{\partial x_j} \left[\left(\mu + \frac{\mu_t}{\sigma_k} \right) \frac{\partial k}{\partial x_j} \right] \quad (3)$$

$$\frac{\partial}{\partial x_j}(\rho \bar{u}_j \omega) = \frac{\gamma}{\mu_t} P_k - \beta \rho \omega^2 + \frac{\partial}{\partial x_j} \left[\left(\mu + \frac{\mu_t}{\sigma_\omega} \right) \frac{\partial \omega}{\partial x_j} \right] \quad (4)$$

While C_μ is the empirical constant in this model and ω , γ and β are the dissipation rate, empirical constant and empirical constant related to the dissipation rate, respectively. In this study SST turbulence model has been utilized due to the similarity of the vortex pumps and centrifugal pumps. This model is a popular model used in CFD to predict turbulent flows which developed by Menter

in the 1990s [28]. SST is a combination the two previous turbulence models and uses the advantages of those models. This model uses a blending function to combine the K- ϵ and K- ω models across the flow domain. This function applies the K- ω model near walls for better accuracy in the boundary layer and the K- ϵ model in the free-stream regions. This approach optimizes accuracy across different flow regimes. In this model a new term for dissipation appears in the equation, represented as *Eq. (5)*:

$$\frac{(1 - F_1)2\rho\sigma_{\omega 2}}{\omega} \left[\frac{\partial k}{\partial x} \frac{\partial \omega}{\partial x} + \frac{\partial k}{\partial y} \frac{\partial \omega}{\partial y} + \frac{\partial k}{\partial z} \frac{\partial \omega}{\partial z} \right] \quad (5)$$

Where the F_1 is the blending function near the wall surface which has been valued by Menter. In regions far from the wall, F_1 is zero. As previously mentioned, the SST model utilizes the value of F_1 to automatically apply the K- ω model near walls and the K- ϵ model in regions farther from the wall.

2.5. Boundary conditions

Boundary conditions play a crucial role in the analysis of a vortex pump to define how the fluid interacts with the pump components and the surrounding environment. Each simulation requires defining boundary conditions to solve the problem. This means that the conditions at the inlet, walls and outlet must be specified. It is assumed that the fluid enters the pump inlet at a pressure of 1atm. As the fluid passes through the impeller, it gains energy and exits with a flow rate of 450 m³/h at the pump outlet. To apply the boundary condition at the outlet, the fluid flow rate is specified in terms of mass flow rate which is defined as follows:

$$\dot{m} = Q \times \rho \quad (6)$$

Where \dot{m} is the mass flow rate, Q is the flow rate and ρ is the density of the fluid. This equation indicates that the mass flow rate is the product of the volumetric flow rate and the fluid's density.

Table 3. Boundary conditions of the simulation

Region	Condition type	Value
Inlet	Total pressure	1 (atm)
Walls	No slip walls	-
Outlet	Mass flow rate	126.375 (kg/s)

Error! Reference source not found. presents a clear and brief overview of the boundary conditions required for the CFD simulation of the vortex pump. The inlet pressure of 1 atm, no-slip walls and outlet mass flow rate of 126.375 kg/s establish a practical framework for analyzing the pump's hydraulic performance. These conditions allow the study to assess how changes in impeller design affect head and efficiency, as explained in later sections. The table is a fundamental part of the

simulation methodology, ensuring that the numerical results are reflect actual operating conditions of the pump while allowing for controlled design optimization. **Error! Reference source not found.** demonstrates the boundary conditions allowed to the pump.

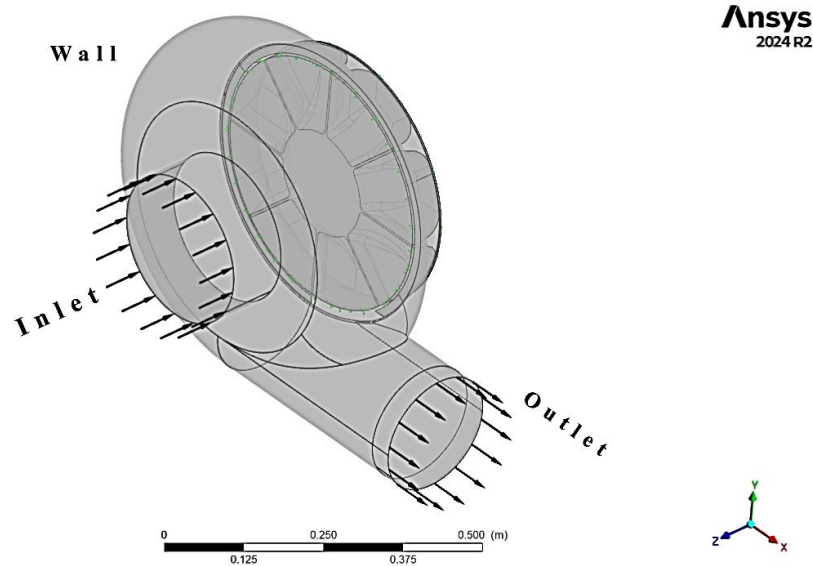


Figure 5. A view of CFX-pre software including settings and boundary conditions

Given that in this simulation the equations are solved numerically, a criterion must be set for stopping the iteration which ensures that when the residuals of the solution fall below the specified threshold, the solver will stop the solution process. This threshold is known as the convergence criterion which is set to 10^{-4} in this simulation. An appropriate time scale in numerical solutions leads to faster convergence in problems and for turbomachinery it is recommended as shown in **Eq. (7)**:

$$T = \frac{2}{\omega} \quad (7)$$

In this equation T is the time scale and ω is the angular frequency. The rotational velocity of the pump is 1230 rpm. Hence. The appropriate time scale for this simulation is obtained at 0.01554. Water has been used as the working fluid to simulate the vortex pump in ANSYS CFX-pre software settings.

3. Simulation options

In this study, several modifications have been applied to the volute and the impeller of the vortex pump to enhance the performance and operational efficiency. These modifications involve geometric refinements to key features including blade design, volute curvature and flow channel dimensions to enhance the hydraulic performance of the pump. The impact of the simulated impeller on overall pump performance has been thoroughly evaluated through detailed computational simulations. Additionally, key parameters including flow rate, head, efficiency and energy losses has been evaluated to determine the impact of these changes. The following sections provide a

detailed explanation of the modifications, designing and the corresponding analysis results. This ensures a comprehensive understanding of the strategies employed to improve the performance of the pump and the outcomes achieved.

3.1. Outlet pipe

To better observe the flow lines at the pump outlet, a pipe with a height of 0.4 m and a diameter matching the outlet has been added to the pump. This addition increases the height difference between the pump inlet and outlet. Figure 6 and Figure 7 show the fluid domain of the vortex pump along with the outlet pipe and the meshing, respectively.

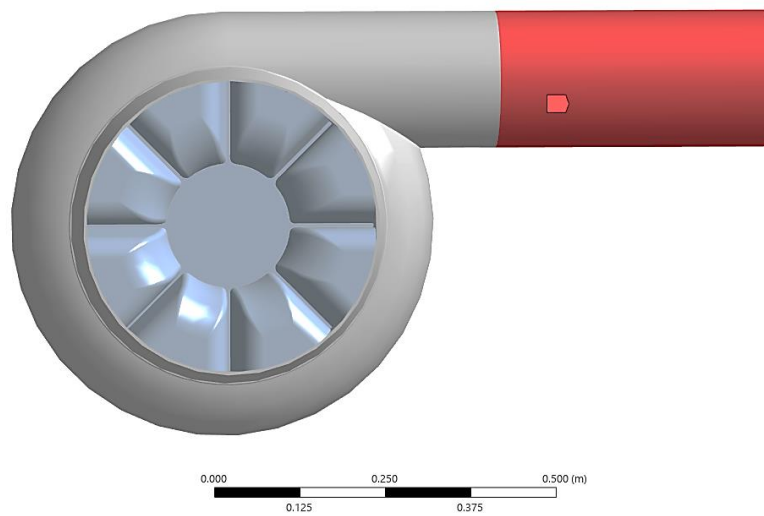


Figure 6. The fluid domain of the vortex pump along with the outlet pipe

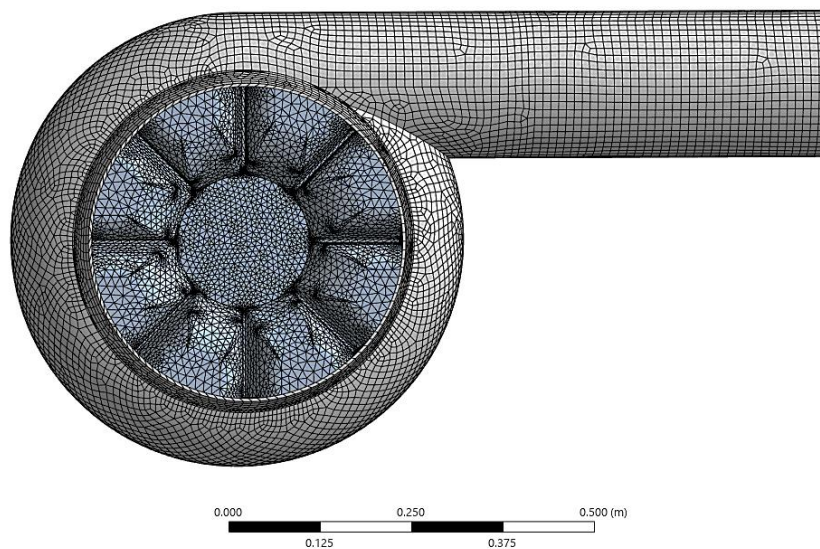


Figure 7. The overall meshing of the pump geometry along with the outlet pipe

In **Error! Reference source not found.**, two different mesh colors are displayed: the blue one represents the impeller mesh and the gray one corresponds to the pump volute and the outlet pipe, it is important to note that this outlet pipe influences the calculation of the pump head.

3.2. Height of leading-edge

In the following, the simulation has been conducted based on increasing the height of the leading edge of the impeller blades to observe the effect on pump performance. To increase the leading-edge height of the blades without altering the original geometry, the blades have been thickened slightly. This ensures that the original impeller geometry remains unchanged despite the increase in leading-edge height. Figure 8 illustrates the changes applied to the impeller.

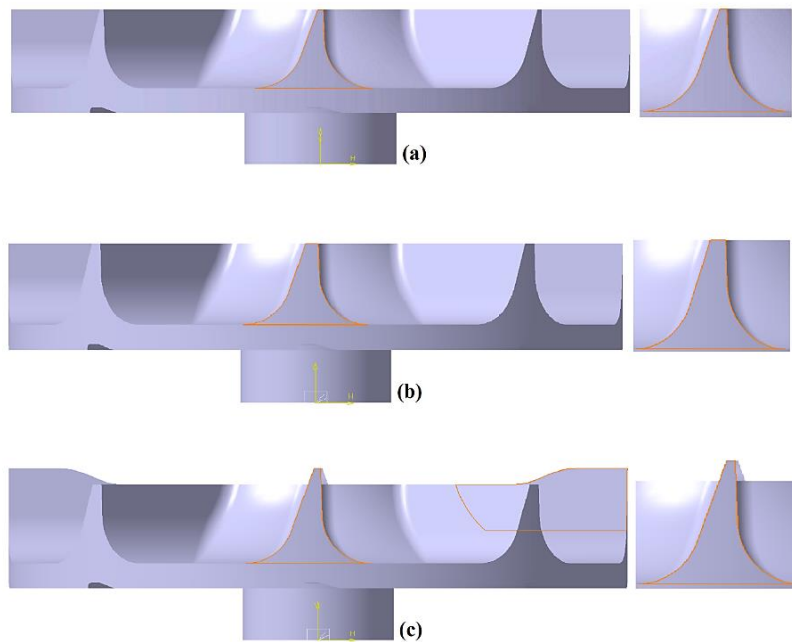


Figure 8. Changes applied to the impeller blades, (a): original impeller, (b): impeller with thickened blades, (c): impeller with blades of increased height

The simulation uses an impeller with thicker blades. In setups with 2 or 4 blades out of 8, the leading-edge height of some blades has increased. Figure 9 illustrates the 8-blade impellers with increased-height blades.

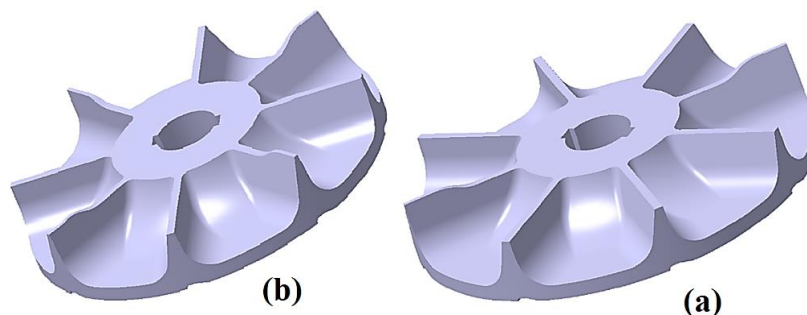


Figure 9. 8-blade impeller, (a): two increased-height blades, (b): four increased-height blades.

To obtain the specifications of a suitable impeller for the studied vortex pump, a simulation has been conducted for another impeller with the same diameter and 12 backward-facing blades. Similar to the previous case, the leading-edge height of some blades has been increased and the results have been analyzed. **Error! Reference source not found.** shows the new 12-blade impeller with different setups.

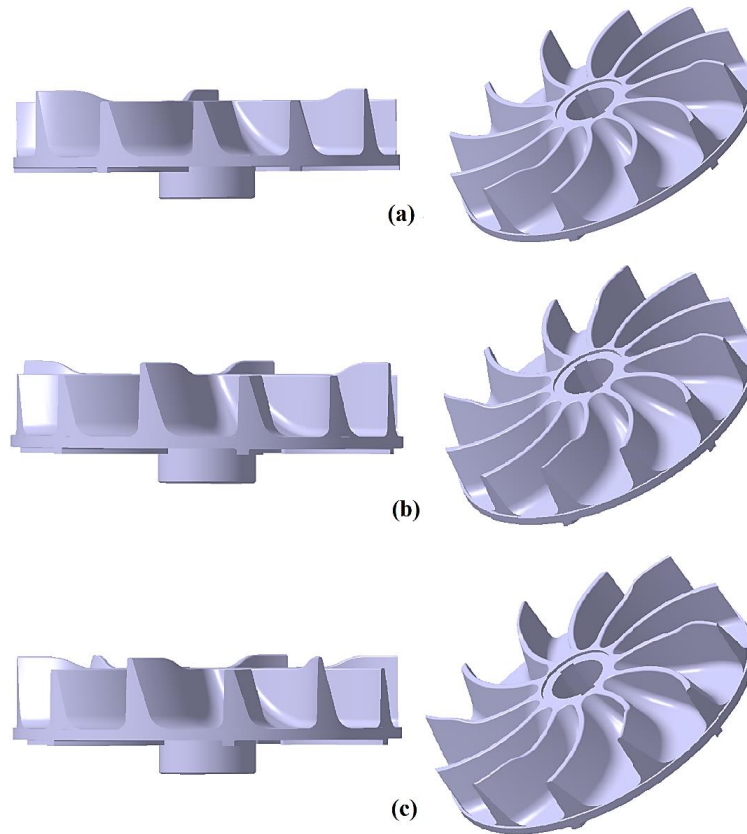


Figure 10. 12-blade impeller with various setups in blades, (a): three increased-height blades, (b): four increased-height blades, (c): six increased-height blades.

4. Results and discussion

The three-dimensional turbulent flow in a vortex pump has been simulated with the SST turbulence model, evaluating a range of operating conditions across various impeller geometries for detailed analysis. This comprehensive study of the pump's performance under different configurations has been performed using CFD to ensure accurate and reliable results. In this section, the results obtained for each impeller are presented and compared with another one and the reference results. The impeller with the best characteristics is introduced as the optimal impeller for the vortex pump. The results have been classified as follows:

4.1. Outlet pipe results

Analysis of the simulation results for the vortex pump with an outlet pipe shows that as the input-output head difference increases, the outlet pressure also rises slightly compared to the basic pump which leads to a higher overall head. Table 4 shows a comparison of the results between the basic pump and the case with an outlet pipe. Figure 11 shows the streamlines and velocity vectors for both cases.

Table 4. Results of vortex pump with different conditions

Case	Outlet pressure (Kpa)	Pump head (m)	Pump efficiency (%)
Basic pump	470.911	38.18	42.99
Pump with outlet pipe	474.7	38.96	43.87

The simulation results of vortex pump in the basic configuration reveal that the head and efficiency values exceed those specified in the pump's specifications. This difference is because of using water as the working fluid in the simulation. In this study, the density of fluid is characterized by mixing the density of water and the solid parts. In fact, the presence of solids also creates more turbulence in the flow which reduces efficiency of the pump. Additionally, solids can partially block flow paths, reducing both the head and flow rate and clog the pump.

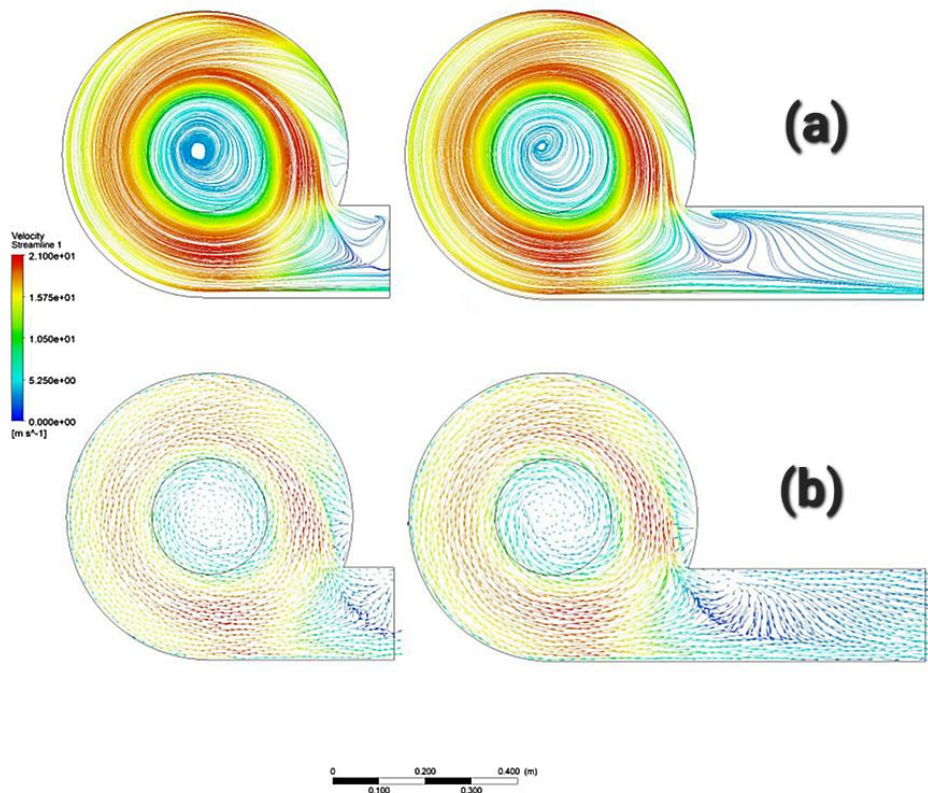


Figure 11. Stream lines and velocity vectors of the basic pump and along with the outlet pipe

Error! Reference source not found. compares the flow patterns between the basic pump (without an outlet pipe) and the pump with an added outlet pipe. The streamline and velocity vector plots reveal significant differences in flow behavior due to the use of outlet pipe. In the basic pump, the flow shows chaotic patterns near the outlet which indicates turbulence and energy losses due to

backflow. In contrast, the pump with an outlet pipe shows smoother streamlines that suggesting improved flow stability and reduced turbulence. The extended pipe helps maintain a more uniform velocity distribution and smoother streamlines, as the fluid gradually decelerates and exits. These flow irregularities not only disrupt the pressure recovery but also contribute to backflow into the volute, reducing the net head and hydraulic efficiency. Scientifically, the key function of the outlet pipe is to extend the downstream boundary condition which allows the fluid to have a superior stability and a aligns the momentum in more distance before exiting. Physically, this addition helps in reducing flow separation and turbulence near the outlet which are typically sources of energy loss. Additionally, the velocity vectors confirm that by indicating a more uniform flow distribution in the pump with an outlet pipe. In this regard, **Error! Reference source not found.** provides quantitative evidence of the performance improvements achieved by the outlet pipe modification. The table compares key metrics including outlet pressure, pump head and efficiency between two configurations. From a hydraulic perspective, the outlet pipe acts as a diffuser by enhancing pressure and reducing kinetic energy losses. It allows the velocity at the pump exit to be more effectively converted into static pressure which contributes directly to the total head. The results indicate that the pump with an outlet pipe achieves a higher outlet pressure, an increased head and a slight efficiency. These physical changes explain the increase in head by 0.78m and efficiency by 0.88% in the simulation results.

4.2. Head - Flow rate

The head-flow rate analysis which is typically shown as H-Q curve, is a fundamental performance characteristic of a pump. It shows the relationship between the head generated by the pump and the flow rate delivered under specific operating conditions. The head of a pump is the height to which the pump can raise a fluid, representing the energy imparted to the fluid. It is typically measured in meters and encompasses components including static head, velocity head and pressure head. Flow rate is the volumetric flow rate of the fluid being pumped, usually measured in liters per second (L/s) or cubic meters per hour (m^3/h). Figure 12 illustrates the head-flow rate curve for all blades.

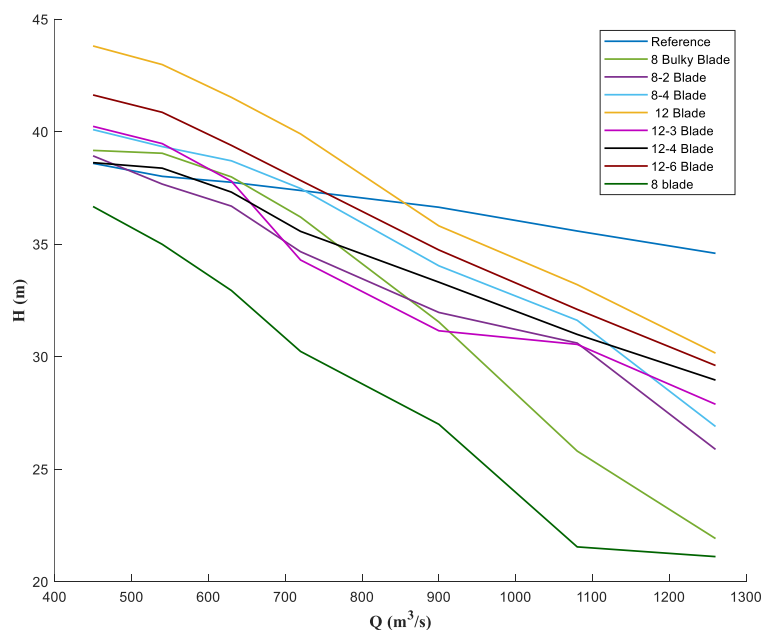


Figure 12. Head – Flow rate results for all geometries

Error! Reference source not found. presents the head-flow rate (H-Q) characteristics for the various impeller configurations tested in the vortex pump. This fundamental performance result reveals several important trends about how different blade designs affect hydraulic performance across the operating range. As expected in centrifugal and vortex pumps, the head decreases as the flow rate increases. This is due to increasing hydraulic losses and reduced pressure generation capability at higher flow rates. The pump must overcome greater resistance from friction and turbulence as more fluid is moved, which reduces the net head produced. All configurations show the typical centrifugal pump behavior where head decreases as flow rate increases. According to the results, the 12-blade backward impeller consistently shows the highest head across the entire range of flow rates. This is because the additional blades provide better reduction of recirculation and maintain a more stable vortex flow pattern within the pump volute. The backward curvature also helps in directing fluid more efficiently toward the outlet, minimizing energy losses. However, the 12-blade backward impeller demonstrates superior performance, maintaining higher head values across the entire flow range compared to other designs. The 8-blade impeller shows the lowest performance, particularly at higher flow rates where the head drops significantly.

The comparison between modified designs yields interesting insights. While increasing the leading-edge height on 50% of the blades in 8-4 configuration impeller provides moderate improvement over the baseline, the simple 12-blade impeller outperforms all modified versions including those with partial height increases. This indicates that the number of blades and the overall impeller geometry have a greater influence on pump performance than by specific alterations in blade height. All configurations show their peak performance at lower flow rates between 0.1-0.15 m³/s, with the performance gap between different designs narrowing as the flow rate increases beyond 0.25 m³/s. The superior performance of the 12-blade design can be attributed to several hydrodynamic factors. The additional blades provide better fluid guidance, reducing recirculation losses and improving energy transfer efficiency. The backward curvature of the blades appears particularly effective in maintaining the vortex structure within the pump chamber. The limited advantages observed from blade height modifications indicate that flow control in vortex pumps depends more on overall blade count and geometry than on localized height adjustments. In fact, excessive height increases might potentially disrupt the balanced vortex flow pattern that is essential for the performance of the pump.

4.3. Efficiency - Flow rate

The efficiency-flow rate curve in pump study, also shown as the η -Q curve, represents the relationship between the efficiency (η) of a pump and its flow rate (Q). This curve is a key tool in analyzing and optimizing pump performance. The results derived from numerical simulations have been plotted for the designed geometries, as shown in Figure 13 for all geometries. From a scientific perspective, pump efficiency is defined as the ratio of hydraulic power (output) to mechanical power (input). As shown in the figure, all impeller designs show a typical efficiency pattern: efficiency increases with flow rate, reaches a peak within a specific optimal range and then declines. This pattern happens because of fluid dynamics and energy losses due to turbulence, friction and recirculation within the pump. Physically, the shape and peak of the results are strongly influenced by the impeller geometry.

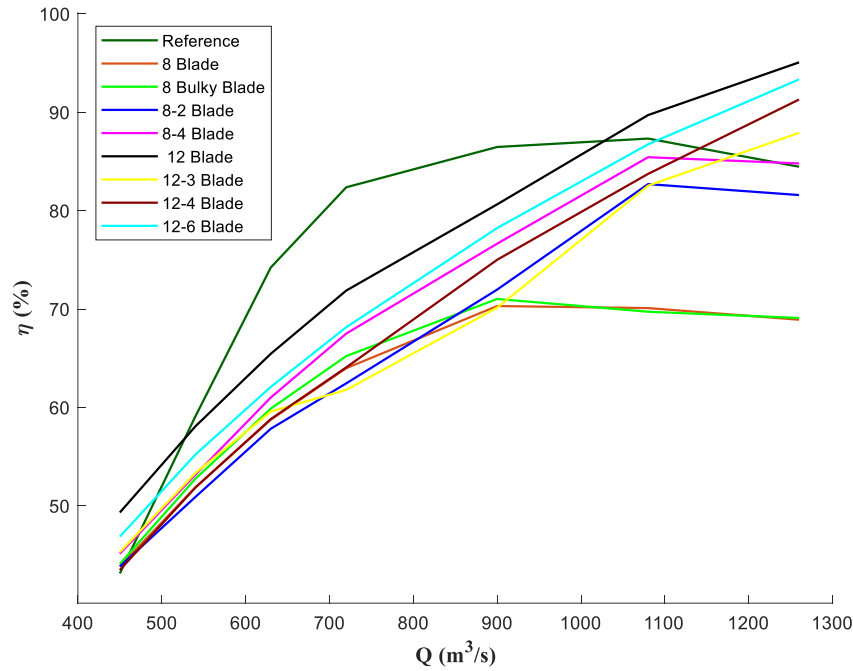


Figure 13. Efficiency-Flow rate results for all geometries

Figure 13 presents the efficiency-flow rate characteristics for the various impeller configurations in the vortex pump. The 12-blade backward-curved impeller demonstrates superior performance and maintaining higher efficiency over a broader flow range. The peak efficiency approaches 95% and outperforms the 8-blade configurations. The increased number of blades improves flow guidance and reduces internal energy losses while the backward curvature supports smoother acceleration and redirection of fluid through the volute. This represents a substantial improvement over the baseline 8-blade configuration which shows significantly lower efficiency values throughout the tested flow rates. The 12-blade configuration particularly outperforms in the optimal flow range of 0.2-0.3 m³/s where it consistently maintains efficiency above 90%. An evaluation of the modified configurations reveals several patterns. The 12-3 blade and 12-4 blade designs show similar efficiency to the standard 12-blade impeller, though with slightly reduced performance. In contrast, the 8-blade fat configuration shows a significant efficiency drop at higher flow rates. The 12-6 blade configuration has a superior efficiency rather than the 8-blade impeller it underperforms compared to the 12-blade configurations. These variations highlight how minor design changes can significantly impact energy performance. The efficiency outcomes exhibit consistent fundamental characteristics across all configurations. All configurations begin with relatively low efficiency values (40-60%) at the minimum flow rate of 0.1 m³/s with performance improving rapidly as flow increases toward the optimal range. Most impellers achieve peak efficiency within a flow range of 0.2–0.3 m³/s. However, few certain configurations such as the 8-blade fat impeller shows significant efficiency drops when operated outside this optimal range. This trend highlights the importance of appropriate pump sizing and system design to optimize operation within the most efficient flow range. These findings have important practical implications for industrial use. The superior performance of the 12-blade configuration makes it a clear choice for applications where maximizing energy efficiency is a top priority. The results also emphasize the operational advantages of maintaining pump operation within the identified optimal flow range (0.2-0.3 m³/s) where efficiency peaks for most configurations.

4.4. Power – Flow rate

Furthermore, the Power-flow rate (P-Q) derived from numerical simulation results have been plotted and presented in Figure 14 for all geometries. This figure represents the relationship between the power input required by the pump and the flow rate it delivers. These results are essential for understanding the energy consumption of the pump under varying operating conditions. Power consumption in a pump system increases with flow rate due to rising hydraulic resistance, higher fluid velocities, and increased friction losses. The mechanical energy supplied by the motor must overcome these resistances to maintain the desired flow, especially in complex internal geometries like those of vortex pumps. Figure 14 presents the power-flow rate characteristics for the various impeller configurations. This approach provides critical insights into the energy consumption patterns across various operating conditions. The results demonstrate a consistent trend where power input increases with flow rate for all configurations. Power input ranges from approximately 40 kW at the lowest flow rates to over 100 kW at maximum capacity. This pattern is typical for centrifugal pumps with higher flow rates need more power to handle the extra hydraulic losses and keep the pump running smoothly.

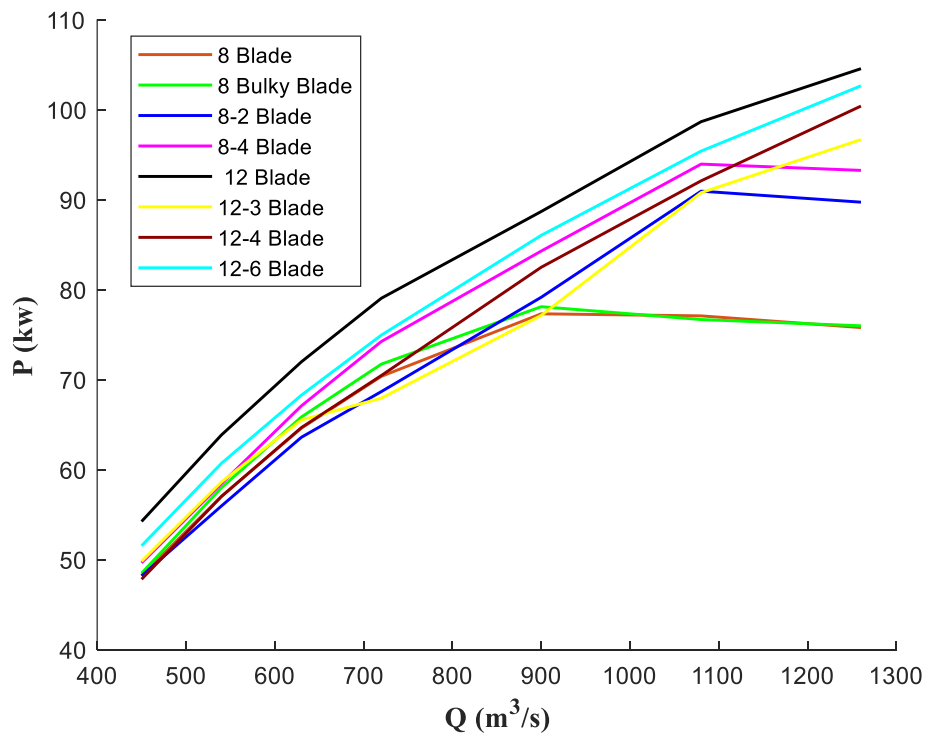


Figure 14. Power-Flow rate results for all geometries

The shape and slope of the P-Q curve are directly influenced by impeller design. In the figure, the 12-blade impeller exhibits the highest power consumption, particularly at higher flow rates, exceeding 100 kW. While this might seem inefficient at first glance, it corresponds with its superior performance in terms of head and efficiency as seen in **Error! Reference source not found.** and **Error! Reference source not found.**. This indicates that the higher energy input is effectively converted into useful hydraulic energy, making the design more powerful and efficient overall.

Other configurations, such as the 8-blade fat impeller, shows a flatter power curve at higher flow rates, suggesting that these designs reach a limit in their ability to transfer additional energy into fluid motion. This behavior implies hydraulic inefficiencies such as flow separation, energy dissipation, or backflow, where additional power does not translate into increased flow or head. The 12-3 and 12-4 configurations show slightly lower power consumption rather than the standard 12-blade configuration, aligning with their moderate efficiency and head values. The standard 8-blade configuration shows a slightly increase in power consumption and highlights the lower hydraulic performance capabilities. At lower flow rates (approximately $0.1 \text{ m}^3/\text{s}$), all configurations exhibit comparable power requirements (40–50 kW) which indicate similar energy demands during startup and low-flow operations. However, as flow rates approach $0.2 \text{ m}^3/\text{s}$, the power curves diverge significantly with the 12-blade designs showing steeper increases that correspond to their enhanced performance capabilities. by increasing the flow rate up to $0.25 \text{ m}^3/\text{s}$, the distinctions become more evident. In certain cases, such as 8-blade fat configuration, the power consumption stabilizes at higher flow rates while others continue to rise. Consequently, all of these results indicate that the impeller with 12 backward-curved blades in its simple form has the highest values of head and efficiency in the simulations. Compared to the reference impeller, the head increased by 4.85m and the efficiency improved by 5.46% under the pump's initial operating conditions.

4.5. Flow rate in vortex pump

In this section, streamlines for various simulated configurations are presented. The results indicate that the fluid flow inside the vortex pump initially impacts the wall near the outlet with a part of the flow subsequently returning to the volute. By increasing the flow rate, the interaction of fluid and volute is reduced and the fluid exits the pump without returning to the volute. Figures 15 and 16 demonstrate the streamline patterns inside the vortex pump for the baseline 8-blade impeller and optimized 12-blade backward-curved impeller, respectively. These figures show how impeller geometry affects the internal flow structure, particularly regarding backflow (a phenomenon where fluid reverses direction and re-enters the volute instead of being discharged efficiently). Backflow leads to increased turbulence, energy losses and reduced hydraulic efficiency.

In the following, as shown in Figure 16, for configurations where the leading-edge of the blades has been extended, the flow pattern closely matches with the baseline impeller with minor differences. However, with the implementation of a 12-blade impeller, the backflow into the volute is considerably reduced. Moreover, replacing the 8-blade impeller with the 12-blade version has led to an improvement in the fluid vortex flow within the pump.

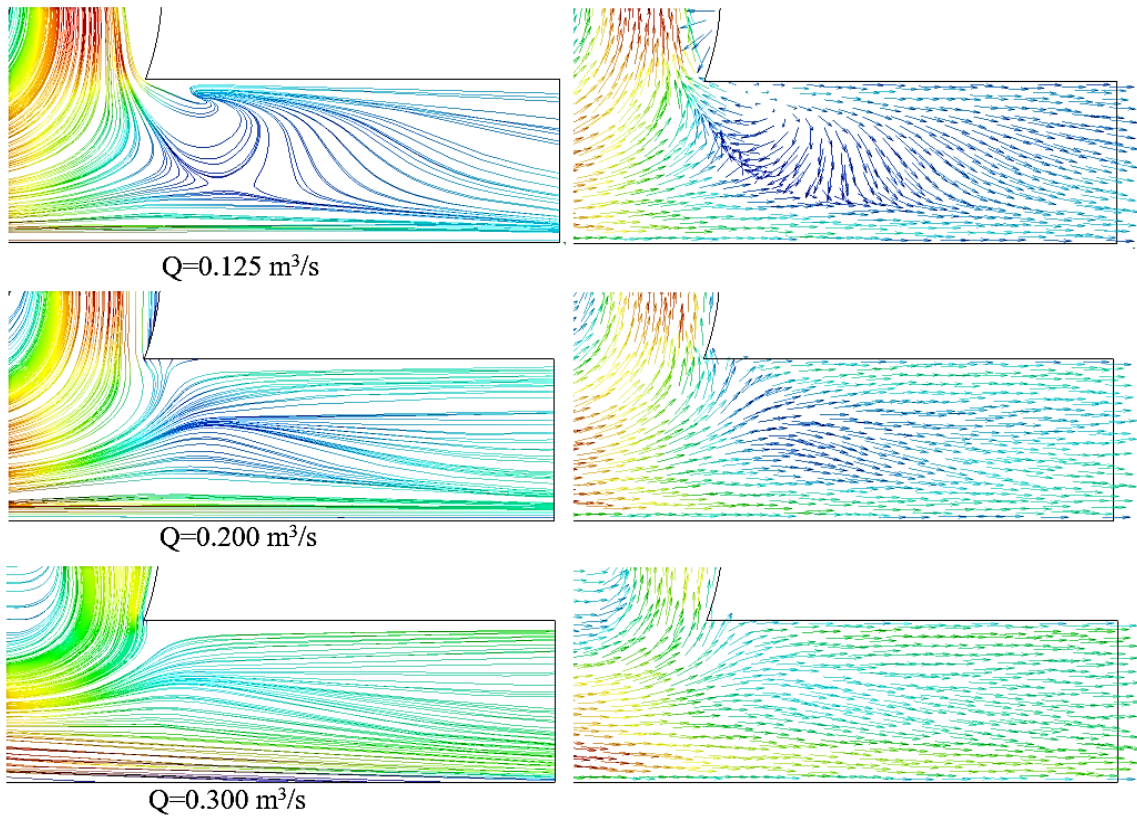


Figure 15. Backflow from the outlet pipe in the vortex pump with the basic impeller

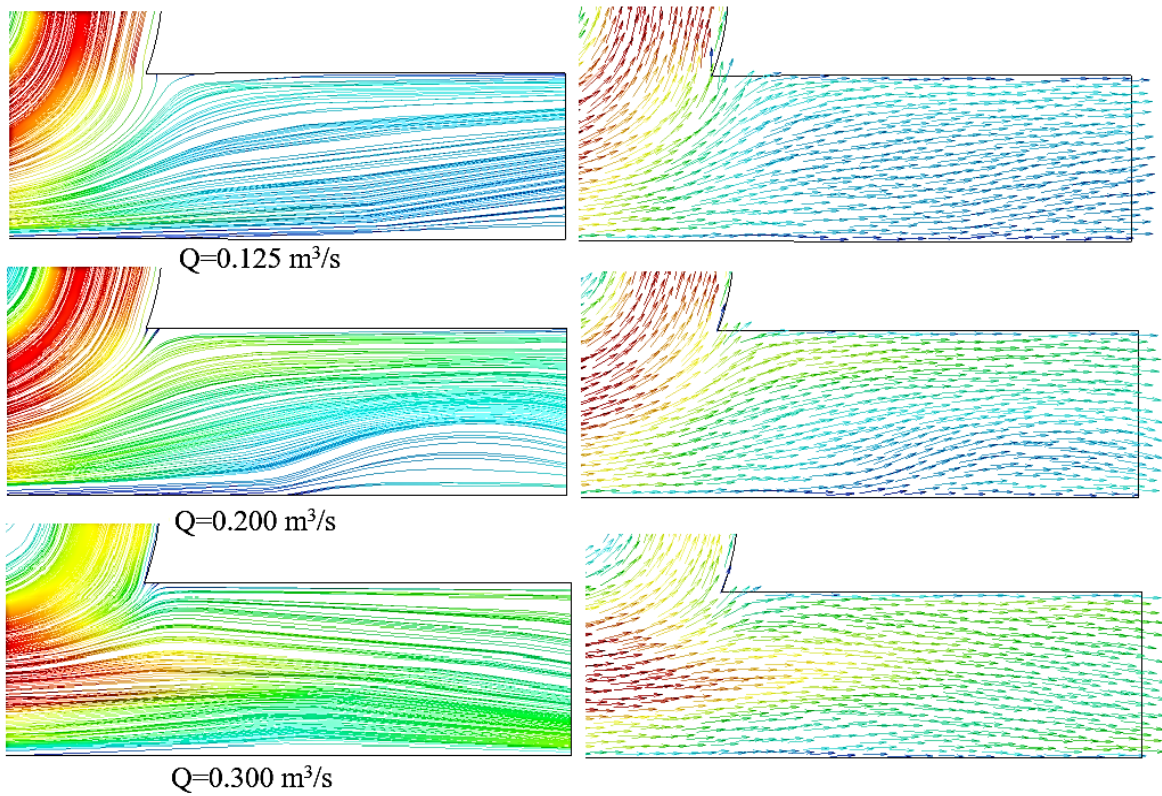


Figure 16. Backflow from the outlet pipe in the vortex pump with an optimized impeller

In Figure 15, the streamlines show significant flow disturbances and recirculation zones near the pump outlet. This chaotic behavior is caused by the limited guidance provided by the 8 straight blades, which fail to direct the fluid smoothly toward the outlet. The high tangential velocity generated by the straight blades contributes to an unstable vortex structure. Physically, this results in energy dissipation, increased wear and a reduction in both head and efficiency. The velocity vectors show distribution with high-velocity regions concentrated near the impeller tips and stagnant zones developing in the volute cavity. Figure 16 presents a more stable and organized flow pattern when using the 12-blade backward-curved impeller. The additional blades offer better coverage and fluid guidance, while the backward curvature reduces the tangential velocity component and promotes more axial flow toward the outlet. The streamlines are more organized and coherent, following smooth trajectories from inlet to outlet with minor flow separation. The backflow observed in **Error! Reference source not found.** is reduced significantly, with nearly all fluid maintaining forward motion through the discharge. These improvements correlate directly with the enhanced performance metrics, as the reduction in flow disturbances performs a higher efficiency and more effective energy transfer.

The comparison between these figures provides valuable insights into the hydraulics of vortex pumps. Blades of the baseline impeller generate tangential velocity components that contribute to flow recirculation, while the backward-curved blades in the optimized configuration more effectively direct the flow axially toward the outlet. The increased blade count in Figure 16 also enhances flow durability by reducing the periodic disturbances related with blade passing in the 8-blade configuration. These observations confirm that impeller geometry significantly influences the fundamental flow mechanisms governing vortex pump performance. The chaotic flow patterns observed in Figure 15 help explain the baseline configuration's greater sensitivity to vibration and wear, whereas the smoother flow in Figure 16 suggests improved mechanical stability. The reduced backflow in the optimized design also implies lower susceptibility to clogging when handling solids, as particles are more likely to be carried completely through the pump rather than recirculating. These factors combine to explain the overall performance advantages of the 12-blade design observed in the quantitative results.

5.conclusion

Vortex pumps are a type of centrifugal pump specifically designed to handle fluids containing solids, fibrous materials, or highly viscous substances. Their unique performance characteristics, compared to conventional centrifugal pumps, have led to widespread adoption across various industries. This study aims to improve the efficiency of vortex pumps, with a primary focus on optimizing the impeller—a key component influencing pump performance. Several impeller designs were simulated and analyzed. The results show that increasing the blade height percentage at the leading edge in the initial impeller design enhanced overall performance. Among the tested configurations, the 12-blade simple impeller produced the best results. This design led to improved internal flow characteristics, resulting in a 5.46% increase in efficiency and a 4.85m gain in head compared to the baseline design. Overall, the findings indicate that variations in the number and angle of impeller blades have a more pronounced effect on pump performance than changes in blade height.

References

- [1] V. Kondus, P. Kalinichenko, and O. Gusak, "A method of designing of torque--Flow pump impeller with curvilinear blade profile," *Eastern-European Journal of Enterprise Technologies*, vol. 3, no. 8–93, pp. 29–35, 2018.
- [2] Y. Song, "Numerical investigation on vortex pump," *Technische Universitaet Berlin (Germany)*, 2021.
- [3] H. Quan, Y. Guo, R. Li, Q. Su, and Y. Chai, "Optimization design and experimental study of vortex pump based on orthogonal test," *Science Progress.*, vol. 103, no. 1, pp. 1–20, 2020.
- [4] M. Tan, K. Zhao, X. Wu, H. Liu, C. Shao, and B. Pan, "Analysis on flow structure in a vortex pump under all flow rates," *Water Supply*, vol. 23, no. 5, pp. 1874–1884, 2023.
- [5] A. Gerlach, P. U. Thamsen, S. Wulff, and C. B. Jacobsen, "Design parameters of vortex pumps: A meta-analysis of experimental studies," *Energies*, vol. 10, no. 1, pp. 1–23, 2017.
- [6] G. P. Schivley and J. I. Dussourd, "An Analytical and Experimental Study of a Vortex Pump," *Journal of Basic Engineering*, vol. 92, no. 4, pp. 889–900, 1970.
- [7] Ohba, H., Nakashima, Y. and Shiramoto, K., 1983. "A study on internal flow and performance of a vortex pump: part 1 theoretical analysis". *Bulletin of JSME*, vol. 26, no. 216, pp.999-1006, 1983.
- [8] A. Gerlach, P. U. Thamsen, and F. Lykholt-Ustrup, "Experimental investigation on the performance of a vortex pump using winglets," In *16th international symposium on transport phenomena and dynamics of rotating machinery (ISROMAC)*, 2016.
- [9] A. Gerlach, E. Preuss, P. U. Thamsen, and F. Lykholt-Ustrup, "Numerical simulations of the internal flow pattern of a vortex pump compared to the Hamel-Oseen vortex," *Journal of Mechanical Science and Technology*, vol. 31, no. 4, pp. 1711–1719, 2017.
- [10] A. Gerlach, S. Wulff, D. Perlitz, F. Lykholt-Ustrup, and P. U. Thamsen, "The optimal vortex pump impeller - An experimental study on clogging behaviour," In *12th european conference on turbomachinery fluid dynamics and thermodynamics. european turbomachinery society*, pp. 1–10, 2017.
- [11] VM Lubieniecki, "Some performance characteristics of a centrifugal pump with recessed impeller," In *Proceedings of the Gas Turbine and Fluids Engineering Conference Products Show, San Francisco, CA, USA*, pp. 26–30, 1972.
- [12] Al-Obaidi, A.R, "Evaluation and investigation of hydraulic performance characteristics in an axial pump based on CFD and acoustic analysis". *Processes*, vol. 12, no. 1, p.129, 2024.
- [13] K. Rutschi, "Die Arbeitsweise von Freistrompumpen (The Operation Principle of Vortex Pumps)," *Swiss Civil Engineering Journal*, vol. 86, no. 32, pp. 575–582, 1968.
- [14] Li, D., Zhang, N., Jiang, J., Gao, B., Alubokin, A.A., Zhou, W. and Shi, J., "Numerical investigation on the unsteady vortical structure and pressure pulsations of a centrifugal pump with the vaned diffuser". *International Journal of Heat and Fluid Flow*, vol. 98, p.109050, 2022.
- [15] Y. Li, G. Feng, X. Li, Q. Si, and Z. Zhu, "An experimental study on the cavitation vibration characteristics of a centrifugal pump at normal flow rate," *Journal of Mechanical Science and Technology*, vol. 32, no. 10, pp. 4711–4720, 2018.
- [16] Y. Y. Su, X. D. Wu, B. Xu, J. H. Feng, T. P. Zheng, and Y. Y. Liu, "Numerical Study on the Hysteresis Effect of Volute Pump with Stay Vanes Based on Vortex Dynamics," In *Journal of Physics: Conference Series*, vol. 2752, no. 1, p. 012139, 2024.
- [17] M. Y. Y. Sha, J. Wang, "Experimental study on internal flow and suction performance of a vortex pump," *Pump Technology*, vol. 4, pp. 9–12, 2003.
- [18] R. Liu, Q. Zhang, S. Zhuang, and K. Wang, "The Influence of the Geometric Parameters of an Impeller on the Transport Capability of Long Flexible Fiber in a Non-Clogging Pump," *Processes*, vol. 12, no. 8, p. 1779, 2024.
- [19] A. Gerlach, "The influence of impeller designs on the performance of a vortex pump," *Technische Universitaet Berlin (Germany)*, 2018.
- [20] K. Zhao, M. Tan, X. Wu, C. Shao, and H. Liu, "Effect of impeller installation position on unsteady flow characteristics of a vortex pump," *Engineering Computations*, vol. 40, no. 2, pp. 335–347, 2023.
- [21] H. Quan, Y. Wu, Y. Guo, K. Song, and Y. Li, "Multiobjective hydraulic design and performance analysis of a vortex pump based on orthogonal tests," *Shock and Vibration*, 2021.
- [22] Gao, X., Zhao, T., Shi, W., Zhang, D., Shi, Y., Zhou, L. and Chang, H, "Numerical investigation of an open-design vortex pump with different blade wrap angles of impeller," *Processes*, vol. 8, no. 12, pp. 1–19, 2020.

- [23] Jiang, L., Wang, W., Shi, Y., Chen, J., Bai, L. and Zhou, L., “Vortex dynamics analysis of an energy loss mechanism in a centrifugal pump impeller”. *Physics of Fluids*, vol. 37, no. 2, p. 025164, 2025.
- [24] Yang, J., Li, X., Cheng, D., Ji, J., Zhao, M., Guo, W. and He, L., “Numerical Simulation for Impeller Structure Optimization for Vortex Pump Based on Orthogonal Design Method”. *Applied Sciences*, vol. 15, no. 5, p.2265, 2025.
- [25] Xin, L., Li, Q. and Liu, Y., “Dynamic analysis of the impeller under optimized blade design for a pump-turbine”. *Journal of Energy Storage*, vol. 107, p.114900, 2025.
- [26] Gao, X., Shi, W., Zhao, R., Zhao, T. and Wang, H., 2021. “Optimization Design and Internal Flow Field Study of Open-Design Vortex Pump”. *Shock and Vibration*, vol. 1, p. 6673200, 2021.
- [27] Wilcox DC. “Turbulence Modeling for CFD”. DCW industries, La Canada. 1998.
- [28] Menter, Florian R. “Review of the shear-stress transport turbulence model experience from an industrial perspective.” *International journal of computational fluid dynamics*, vol. 23, no. 4, pp. 305-316, 2009.